GNSS TOMOGRAPHY OF THE ATMOSPHERE - EXPECTATION FROM GALILEO FOC

Gregor Möller, Robert Weber, Johannes Böhm

Vienna University of Technology, Department of Geodesy and Geoinformation, Gußhausstraße 27-29, 1040 Vienna, Austria, gregor.moeller@tuwien.ac.at

ABSTRACT

The aim of this paper is to investigate the impact of the upcoming Galileo system on GNSS tomography. The area covered by our tomography model is limited to the Austrian territory. The GPS and GLONASS data of 12 sites in different environments are analysed with respect to its quality and impact on the atmospheric tomography approach. We show how additional Galileo observations help to close the lack of data and therewith to improve the quality of the derived refractivity field. The Galileo constellation (26 satellites as planned to be active in 2015) is simulated by a signal generator which is able to provide Galileo E1 observations in RINEX format.

1. INTRODUCTION

GNSS observation data allow recovering the structure of the atmosphere. In particular the temporal and spatial distribution of the high variable water vapor in the lower layers of the atmosphere (up to 12 km) is of interest for regional weather forecast and precise positioning. In order to obtain this information above Austria the atmosphere is divided into a 3D voxel-model, see Fig. 1-1. The spatial and vertical resolution of the voxel model is fitted to ALARO5-Austria – the operational limited area model at ZAMG (Austrian Federal Office for Meteorology and Geodynamics, www.zamg.ac.at).

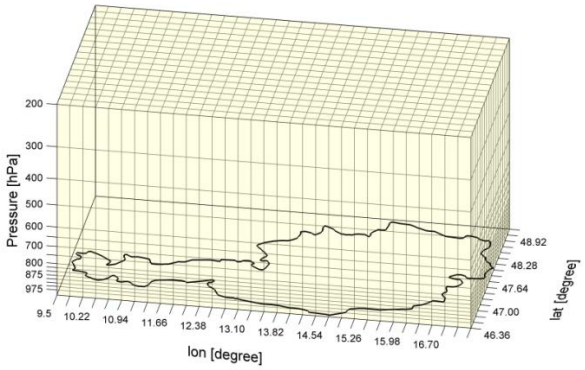

Figure 1-1, 3D voxel structure with a spatial resolution of 0.16° lat (~17.8 km) x 0.24° lon (~18.0 km) and 16 pressure levels. A pressure value of 200 hPa corresponds to a height of about 11800 m.

In order to recover the wet refractivity N_{wet} in each voxel an atmospheric tomography approach is applied.

Figure 2-2, Meteorological Sensor Network in Austria

Input data are slant wet path delays from GNSS observations. The approach to obtain slant wet path delays (SWD) is described by Eq. 1

$$SWD = \left[\frac{\Delta\rho_{apr}}{m_h(e)} + \frac{\Delta\rho_{corr}}{m_w(e)} - ZHD\right] \cdot m_w(e) + PZDR \quad (1)$$

where $\Delta\rho_{apr}$ is the dry component of the tropospheric delay calculated by the Global Pressure Temperature model GPT [1], using pressure values derived from 10 years ECMWF data. The correction term $\Delta\rho_{corr}$ is estimated in an adjustment process every 15 min. Both are mapped to zenith using the dry $m_h(e)$ and wet $m_w(e)$ Global Mapping function GMF [1]. To obtain only wet delays in zenith direction, the hydrostatic delay has to be subtracted. Therefore atmospheric pressure values p_0 at the antenna reference point are extrapolated from meteorological sensors nearby, see Fig. 1-2. They are used in Eq. 2 to calculate the zenith hydrostatic delay. Afterwards the zenith wet delay is mapped to a certain elevation angle by the wet GMF to obtain isotropic SWD.

$$ZHD = \frac{(0.0022768 \mp 0.0000005)\cdot p_0}{f(\varphi,H)} \quad (2)$$

The azimuthal-anisotropic part of the slant wet delay is described by the term PZDR (Pseudo-Residuals). It can be obtained directly if the GNSS observations are processed undifferenced or it can be recovered from Double Difference Residuals (DDR) if they are normally distributed, see „Zero Mean assumption“ in [2].

In order to reconstruct the wet refractivity N_{wet} from a large number of SWD we make use of the relation:

$$A \cdot x = m \tag{3}$$

where the vector m represents the observations and x describes the current state of the atmosphere, i.e. the refractivity $N_{wet,j}$ in each voxel j. The matrix A defines the mapping of the state x on the observations m. The matrix elements a_{ij} of A are the subsections of the i^{th} slant path in the j^{th} grid cell. Matrix A is defined by the voxel structure of the tomography model. If the ray bending is neglected and the slant path is assumed to be straight we obtain a linear inverse problem for the determination of x. The matrix A in GNSS tomography is most frequently not squared, ill-posed and ill-conditioned. Hence, to invert the A matrix is rather tricky. Different approaches have been developed to solve this problem like the usage of constraints, the iterative algorithm technique, a Kalman-filter, the Singular Value Decomposition or the least squares (LSQ) approach, see [3], [4] or [5]. Independent from the reconstruction technique a high station density would provide an enhanced resolution (especially in vertical direction) and would help to reduce the poor results at the lower tropospheric levels and at the boundaries of the chosen testbed. Additional Galileo observation might help to close the lack of data. In order to study the impact of upcoming Galileo observations on the tomography approach a full operational capability (FOC) is simulated and analysed.

2. TESTBED

Our studies are supported by data of the Austrian GNSS reference network EPOSA (Echtzeit Positionierung Austria, www.eposa.at). Fig. 2-1 gives an overview about the GNSS stations which are currently operated. From this network we formed two sub-networks of six sites each - highlighted in blue - in order to test the impact of different conditions on the GNSS tomography approach.

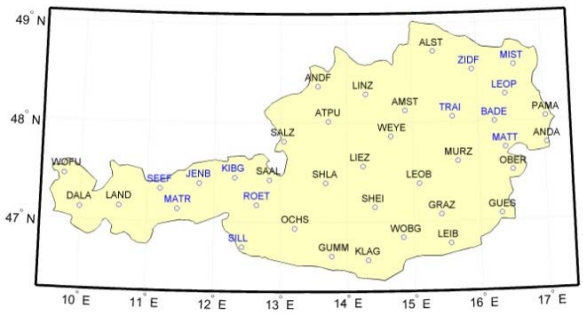

Figure 2-1, Map of the Austrian GNSS Reference Network EPOSA

The mean inter-station distance is about 40 km, the ellipsoidal heights vary for sites in the rather flat region of East-Austria between 220 m and 410 m and for the sites in the mountainous region of West-Austria between 600 m and 2220 m. Fig. 2-2 shows the skyplot for site Leopoldau *(*LEOP) and Jenbach (JENB) together with station residuals for the L2 carrier phase. The residuals are derived from the real-time network solution – estimated from the EPOSA reference network provider over 7 days in September 2013.

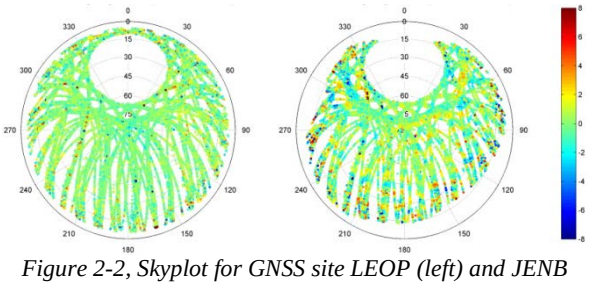

Figure 2-2, Skyplot for GNSS site LEOP (left) and JENB (right). L1 GPS+GLONASS residuals (mm) are color-coded

JENB shows the typical behaviour of a mountainous site with obstructions and a noisier residual field - especially at low elevation angles. This might influence the number and the quality of the derived SWD. To obtain the number of observations daily (24 hour) RINEX data with 30 second sampling rate are analysed. By assuming a cut off elevation angle of five degrees on average 48000 observations on L1 at each site (25700 GPS - and 22300 GLONASS observations) are obtained. Fig. 2-3 shows the number of GPS and GPS+GLONASS satellites in view at site LEOP over the time period of 24 hours. It varies between 7 to 13 GPS satellites and 6 to 10 GLONASS satellites. For sites with more obstructions like JENB on average one satellite less is observed which leads in total to about 15% fewer observations.

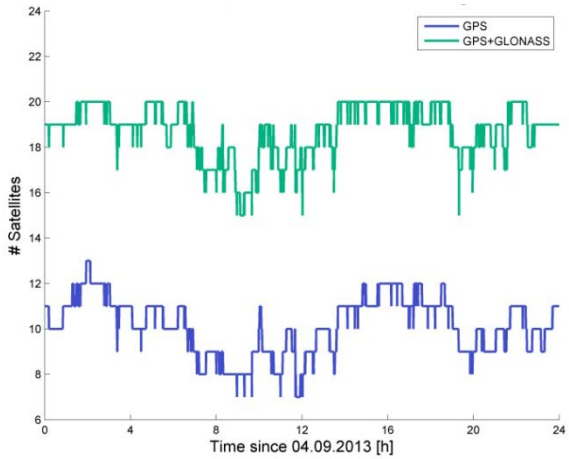

Figure 2-3, GPS & GLONASS satellites in view above 5° elevation angles at site Leopoldau (LEOP) - derived for 4th September 2013

3. GALILEO FOC

In an initial step a full constellation of active satellites in

a 27/3/1 Walker constellation was simulated with almost circular orbits (a = 29600 km, e = 0.009, i = 56°) – using the signal generator NAVx-NCS Professional from Ifen Gmbh (www.ifen.com). By assuming a cut off angle of five degrees at site LEOP on average nine satellites are visible at the same time. Fig. 3-1 shows the number of satellites in view over 24 hours. The number of satellites in view varies between 6 and 11 satellites.

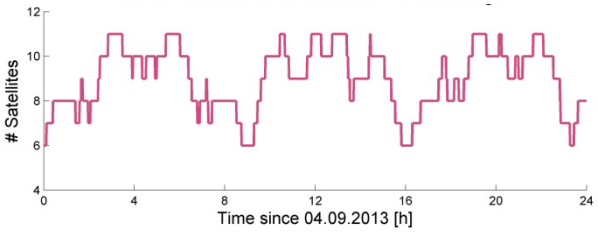

Figure 3-1, Galileo satellites in view above 5° elevation angles at site (LEOP)

Combing the observations from GPS and GLONASS over a period of 15 minutes leads on average to 170 observations at one GNSS site. By Galileo FOC additional 90 observations in new azimuth and elevation angles could be added. Thus the distribution of slant path delays becomes more homogeneous. Temporal variations (due to less satellites in view) can be widely compensated and the solution of the Eq. (1) would become more stable.

4. VOXEL TRAVERSAL

The wet refractivity N_{wet} in a voxel can only be estimated if the connecting line between site and GNSS satellite passes this voxel. In order to assess the number of passed and empty voxels the voxel model is fitted to the two sub-networks in the manner that the model covers the surface area spanned by the six GNSS sites in each cluster, see Figure 4-1.

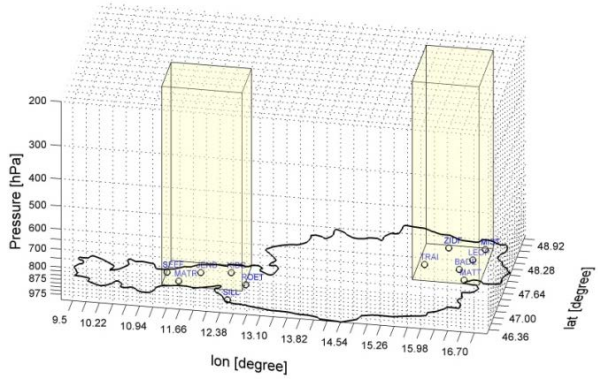

Figure 4-1, 3D voxel size above East and West Austria with a spatial resolution of 0.16° lat (~17.8 km) x 0.24° lon (~18.0 km) and 16 pressure levels

From each GNSS site the Cartesian coordinates are known. The GPS and GLONASS broadcast message allows to compute the satellite positions with meter accuracy. The unit vector of every site-satellite-pair gives the direction to the satellite. Both, the site coordinates and the directions are input for the voxel traversal algorithm, see [6]. This algorithm is used to detect voxel traversals. Fig. 4-2 shows the traversals of the slant pathes of the GPS satellite PRN01 at a single epoch.

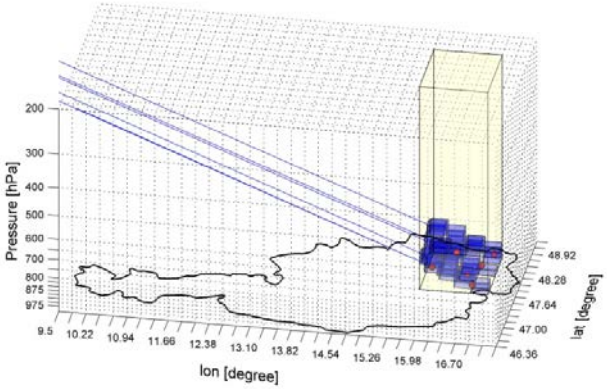

Figure 4-2, Voxel traversal event for GPS satellite PRN01 in view. The slant pathes are assumed as straight lines

The voxel traversal algorithm is applied to each satellite in view over the time period of 15 minutes. In a first run with GPS observations about 55% of the voxels are covered. If GLONASS and Galileo observations are added, the proportion of remaining empty voxels can be reduced to <15% with a variation of 8% over time due to the varying number of satellites in view and the changing satellite geometry during the observation periods.

5. OUTLOOK

As described in this paper a Galileo FOC constellation would provide a significant amount of additional slant pathes which helps to reduce the number of empty voxels. Nevertheless, on the basis of single slant wet delays it is quite difficult to localise the correct N_{wet} in each voxel. Hence we are going to analyse the number of intersection points, i.e. two or more slant pathes crossing the same voxel. Remaining lacks should be closed by low cost single frequency receivers – well-positioned inside or if possible in the surrounding of the existing GNSS network. The potential of using GPS L1 receivers therefore is currently reviewed in the project GNSS-ATom which is funded by the Austrian Research Promotion Agency (FFG). In addition, the Austrian network provider establishes a new data stream with all GPS and GLONASS observations below five degrees. Dependent on the obstructions at each site it would increase the number of intersection points at lower layers of the atmosphere. A detailed analysis is envisaged.

6. REFERENCES

1. Böhm, J., Heinkelmann R. & Schuh H. (2007). Short Note: A global model of pressure and temperature for geodetic applications. *Journal of Geodesy*. doi:10.1007/s00190-007-0135-3.
2. Alber, C. Ware, R., Rocken, C., & Braun, J. (2000). Obtaining single path phase delays from GPS double differences. *Geophysical Research Letters*, 27, pp2661-2664.
3. Bender, M., Stosius, R., Zus, F., Dick, G., Wickert, J., Raabe, A. (2011). GNSS water vapour tomography – Expected improvements by combining GPS, GLONASS and Galileo observations. *Advances in Space Research*, 47, pp886-897.
4. Rohm, W. (2012). The ground GNSS tomography – unconstrained approach. *Advances in Space Research*, 51, pp501-513.
5. Perler, D., Geiger, A., & Hurter, F. (2011). 4D GPS water vapor tomography: New parameterized approaches. *Journal of Geodesy*, 85, pp539-550
6. Amanatides, J., Woo, A. (1987). A Fast Voxel Traversal Algorithm for Ray Tracing, *Proc. Eurographics '87, Amsterdam, The Netherlands, August 1987*, pp1-10.